Proceedings of the 4th International Conference on Materials Chemistry and Environmental Engineering
DOI: 10.54254/2755-2721/63/20241005

Hierarchical porous carbon with abundant N/O doping as an anode for zinc ion hybrid supercapacitors

Yuchen Li[1], Shun Yang[1], Penghao Chai[1], Jianghuan Li[1], Qiulong Guan[1], Lixia Bao[2], Xin Li[1,3,4], Jiong Peng[1,3,5], Wensheng Deng[1,3,6]

[1]School of Chemistry and Chemical Engineering, Beijing Institute of Technology, Beijing, 100081, China
[2]Analysis & Testing Center, Beijing Institute of Technology, Beijing, 100081, China
[3]Corresponding author

[4]klkxlx@163.com
[5]jiongpeng@163.com
[6]huagong@bit.edu.cn

Abstract. Aqueous zinc-ion hybrid supercapacitors (ZISCs) known for their affordability, stability, and high energy density represent innovative energy storage devices. Porous carbon is usually used as the cathode material of ZISCs, and its structure significantly affects the dual performance of high power density and energy density of ZISCs. Herein, a one-pot carbonization strategy is proposed, eliminating the need for templates, additional heteroatom compounds, and activation processes. By precisely controlling the temperature to optimize the structure and electrochemical performance of carbon materials, we successfully synthesized hierarchical porous carbon materials (NOPC-800) with a high specific surface area of 1545.7 m^2g^{-1}, featuring dual doping of 12.3 at% nitrogen and 13.35 at% oxygen. The self-doping of abundant nitrogen and oxygen atoms facilitates the chemical adsorption of ions and accelerates pseudocapacitive reaction kinetics. Leveraging these advantages, ZISCs were assembled using NOPC-800 as the positive electrode and zinc as the negative electrode, showcasing remarkable performance: a specific capacity of up to 121.9 mAh g^{-1}, an energy density of 97.5 Wh kg^{-1}, and a power density of up to 16000 W kg^{-1}. Remarkably, NOPC-800 maintained an excellent capacity retention of 94.9% after 10,000 cycles at a current density of 10 A g^{-1}. This research paves an innovative and feasible path for the design and advancement of novel heteroatom-rich carbon cathodes.

Keywords: Zinc-ion hybrid supercapacitors, carbon material, rich N/O-doping, hierarchical porous structure

1. Introduction

Metallic zinc is regarded as an ideal negative electrode material for aqueous energy storage devices due to its high theoretical capacity (820 mAh g^{-1}), low potential (0.76 V vs the standard hydrogen electrode), high hydrogen evolution overpotential, and cost-effectiveness. In recent years, a substantial amount of research effort has been focused on zinc-based aqueous energy storage devices. Among these, Aqueous zinc-ion hybrid supercapacitors (ZISCs) composed of a zinc negative electrode and a carbon positive electrode possess the advantages of both supercapacitors and batteries, making them a promising and

DOI: 10.54254/2755-2721/63/20241005

efficient energy storage device [1-3]. On one hand, the carbon cathode, owing to its adsorption/desorption charge storage mechanism, undergoes no phase transition and theoretically possesses an exceptionally long cycle life. On the other hand, the zinc anode exhibits the faradaic reaction with an infinite theoretical capacity, allowing for the maximization of the double-layer capacitance of the carbon cathode. Furthermore, in comparison to aqueous energy storage devices employing electrolytes with lithium, sodium, or potassium salts, using a zinc salt solution as the electrolyte confers a significant advantage: the heightened hydrolytic ability of Zn^{2+}. Taking a 2 M $ZnSO_4$ electrolyte as an example, the solution turns acidic (pH≈3.6) due to the hydrolysis of Zn^{2+}, resulting in the substantial release of H^+. Research indicates that when porous carbon serves as the positive electrode material for ZISCs, both Zn^{2+} adsorption and H^+ adsorption onto the carbon material surface contribute to the energy storage process. Given the smaller radius and lighter relative atomic mass of H^+ compared to Zn^{2+}, H^+ emerges as an attractive charge carrier. Therefore, in the design of ZISCs positive electrode materials, consideration should be given not only to the Zn^{2+} storage process but also to the crucial aspect of H^+ storage. However, due to the limited ion adsorption capacity of the carbon cathode, the charge storage capacity is insufficient, resulting in the observed lower energy density of reported ZISCs devices compared to expectations. Designing porous structures and heteroatom (N, O, P, and S) doping are considered to be effective strategies for improving the electrochemical performance of ZISCs, the porous structure provides abundant adsorption/desorption sites and rapid transfer channels for electrolyte ions. Heteroatom doping can not only adjust the local electronic structure to increase the material's adsorption capacity for electrolyte ions but also trigger a reversible redox reaction to provide additional pseudocapacitance, increasing energy density without affecting the inherent power performance and cycle life of the carbon cathode. Regrettably, as highlighted in the majority of research reports, substantial heteroatom doping of carbon materials typically necessitates the use of a significant quantity of additional heteroatom dopants and templates. The associated costs of this method are high, and the operational procedures are intricate, posing obstacles to the widespread adoption of carbon-based heteroatom-doped supercapacitors (ZISCs) in practical applications. Consequently, there is an urgent need to explore a novel, straightforward, and expeditious method for achieving widespread heteroatom doping within carbon structures. This endeavor is instrumental in advancing the commercialization of ZISCs.

In this work, a template-free one-pot carbonization strategy was introduced, utilizing melamine, citric acid, and zinc chloride as precursors, leading to the successful synthesis of hierarchical porous carbon material doped with abundant N (12.3 at%) / O (13.35 at%) through hydrothermal cross-linking, carbonization, and acid washing. The advanced NOPC-800 cathode not only provided ample active sites for Zn^{2+} and H^+ storage but also facilitated substantial ion transport channels, thereby achieving rapid ion transfer kinetics. A systematic analysis was conducted on the influence of temperature on the material's structure, morphology, and electrochemical performance when integrated into ZICSs. The optimized NOPC-800 demonstrated outstanding electrochemical properties, including a remarkable specific capacity of 121.9 mAh g^{-1}, a substantial energy density of 97.5 Wh kg^{-1}, and a notable power density of 16000 W kg^{-1}. Even after 10,000 cycles at 10 A g^{-1}, the capacity retention remained exceptionally high at 94.5%, highlighting its remarkable cyclic stability. This research presents a novel and viable approach for the design and exploration of new carbon cathodes.

DOI: 10.54254/2755-2721/63/20241005

2. Experimental Procedures

2.1. Synthesis of NOPC materials

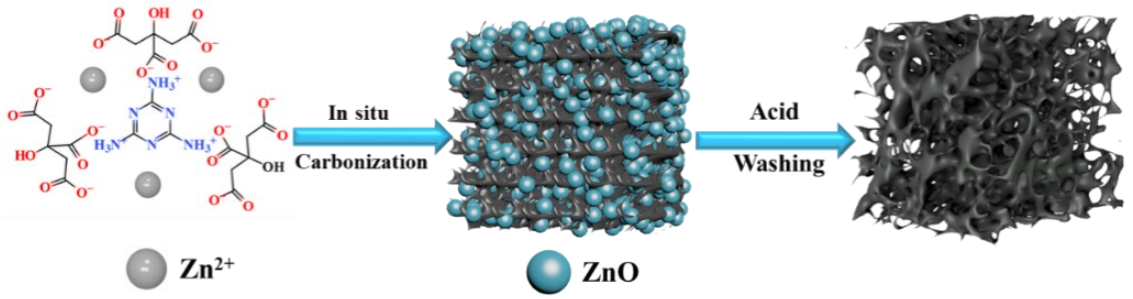

Figure 1. Schematic diagram of the preparation process of NOPC materials

The synthesis schematic of NOPC materials is illustrated in Figure 1. Initially, a mixture of 3 g zinc chloride, 1.92 g citric acid, and 1.26 g melamine was dissolved in 100 mL deionized water and stirred at room temperature for 3 hours until achieving homogeneity. Subsequently, the solution was dried at 120 ℃, and the resulting material was ground into powder to serve as the carbon precursor. The precursor was then carbonized in an argon atmosphere, ramping up the temperature at a rate of 5 ℃/min to reach 600, 700, 800, and 900 ℃, respectively. Finally, the samples underwent hydrochloric acid etching and acid washing to remove ZnO generated during the carbonization process. The resulting product is an N/O co-doped hierarchical porous carbon material. The samples were designated as NOPC-600, NOPC-700, NOPC-800, and NOPC-900, corresponding to the different carbonization temperatures.

2.2. NOPC Materials characterizations

Scanning electron microscopy (SEM, JSM-7500F) was used to observe the micromorphological structure of the prepared samples. The structural information of materials was characterized by Raman spectrum (Renishaw Invia) using 514 nm laser excitation under ambient conditions and XRD patterns (Bruker D8, Germany) with a Cu Kα radiation source. Nitrogen adsorption/desorption measurements were performed using a Micromeritics ASAP2020 physisorption analyzer at −196 ℃. The specific surface area and pore size distribution were evaluated by using the Brunauer−Emmett−Teller (BET) equation and the nonlocal density functional theory model. The carbon surface chemistry was revealed using an X-ray photoelectron spectrometer (XPS, AXIS Ultra DLD).

2.3. Electrochemical Tests

The working electrodes were prepared by pressing a slurry mixture consisting of NOPC materials (80 wt%), polytetrafluoroethylene (PTFE, 10 wt%), and Super P (10 wt%) onto the stainless-steel mesh and then dried at 80°C overnight (the mass loading of active carbon substance is 2 mg cm^{-2}). The aqueous Zn-ion hybrid capacitors (ZISCs) were assembled in a CR2025-type cell, with the working electrode serving as the cathode, a 2M $ZnSO_4$ solution as the electrolyte, a Whatman filter paper as the separator, and high-purity Zn foil (with a thickness of 100 μm, Zn content >99.99%) as the anode. The galvanostatic charge/discharge (GCD) characterization was conducted using a LAND CT3002A battery test system within the potential range of 0 to 1.8 V. The cyclic voltammetry (CV) and electrochemical impedance spectroscopy (EIS) tests were studied on a CHI660E electrochemical workstation. The specific capacity (C, mAh g^{-1}) was calculated based on the GCD profiles using the following equation:

$$C = \frac{I \times \Delta t}{m} \tag{1}$$

DOI: 10.54254/2755-2721/63/20241005

where I (A g^{-1}) is the current density, t (s) is the discharging time, and m (g) is the mass loading of the active substance on the cathode.

3. Results and discussion

3.1. Characterization analysis of morphology and structure of NOPC samples

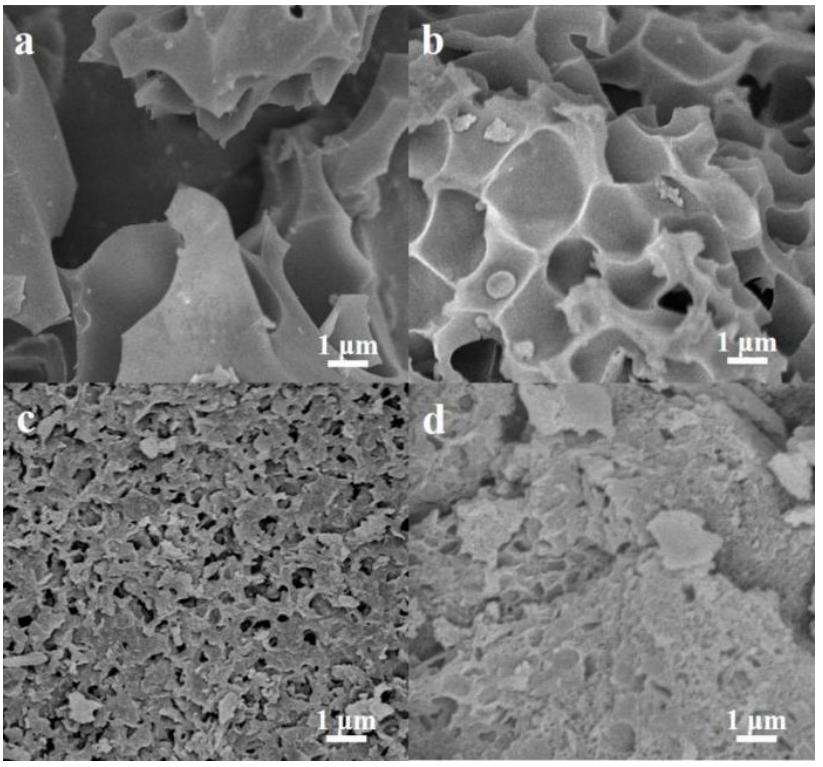

Figure 2. SEM images of samples at different temperatures: (a) NOPC-600, (b) NOPC-700, (c) NOPC-800, (d) NOPC-900.

To investigate the impact of temperature on the morphological structure, SEM was employed to observe the micromorphology of samples at different temperatures. As depicted in Figures 2a and 2b, NOPC-600 and NOPC-700 are primarily composed of open pores and shallow pores due to incomplete carbonization resulting from a relatively low calcination temperature. The larger diameters of these pores pose challenges in providing sufficient ion adsorption sites and storage space. When the carbonization temperature is 800°C, NOPC-800 exhibits an interconnected hierarchical porous structure (Figure 2c), which is expected to achieve excellent electrochemical performance. However, with a further increase in temperature to 900°C, the structure of the carbon material becomes unstable, and a significant amount of zinc oxide etches the carbon skeleton during the reduction process. Consequently, the interconnected carbon walls are partially destroyed, leading to thicker pore walls, gradual disappearance of pores, and unsuitability for ion diffusion and transfer (Figure 2d). NOPC-800 demonstrates a well-defined pore structure owing to the appropriate carbonization temperature. These interconnected pores not only offer abundant active sites for ion storage but also reduce ion diffusion distance and enhance charge transfer[4], making it an ideal electrode material.

DOI: 10.54254/2755-2721/63/20241005

3.2. Characterization analysis of morphology and structure of NOPC samples

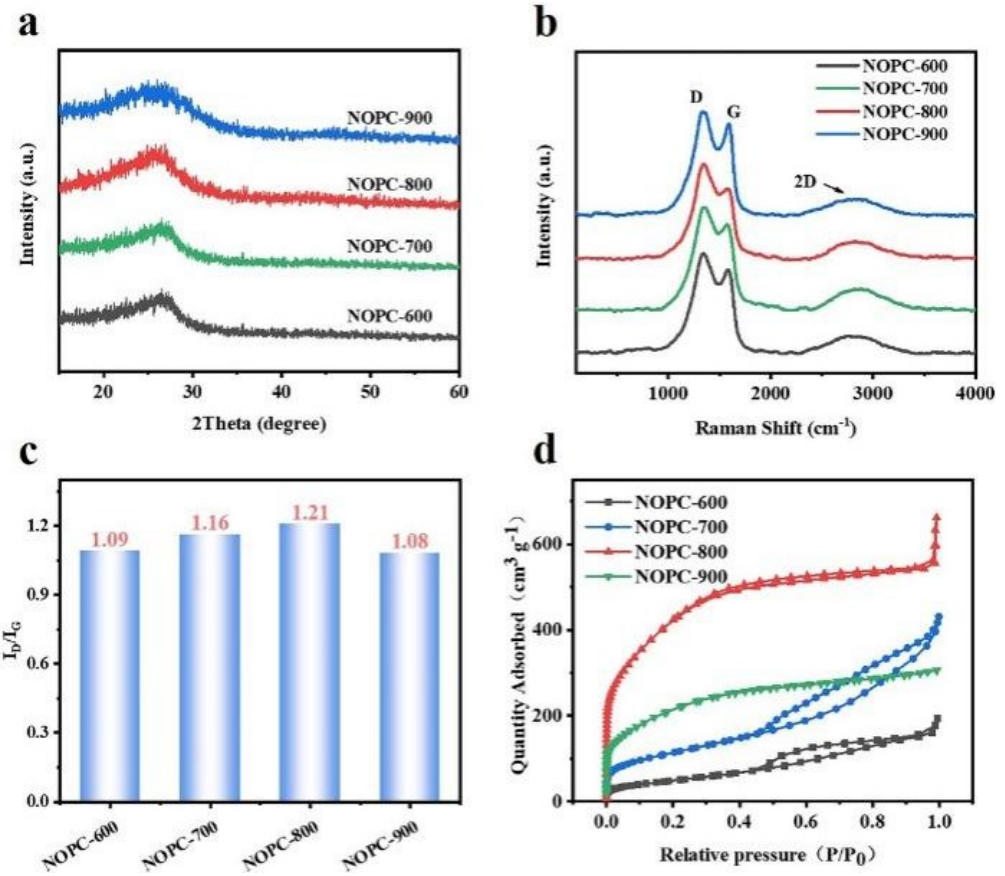

Figure 3. (a) XRD spectrum, (b) Raman spectrum, (c) I_D/I_G value bar chart, and (d) N_2 adsorption-desorption curve of samples at different temperatures.

XRD patterns were employed to confirm the structural characteristics of the prepared carbon samples. As depicted in Figure 3a, all samples exhibit a single broad diffraction peak centered primarily at 23.7°, corresponding to the (002) crystal plane of amorphous carbon. With an increase in pyrolysis temperature from 600 ℃ to 900 ℃, the (002) peak widens, and the angle decreases. This change indicates that the interlayer distance of the carbon material becomes larger, and the structure becomes more disordered, which corresponds to the SEM images. Raman spectroscopy was employed to further evaluate the defects and amorphous structure of the samples. The two peaks located near 1346 cm^{-1} and 1579 cm^{-1} respectively represent the D peak characteristic of sp^3 defects in carbon materials and the G peak characteristic of sp^2 ordered graphite (Figure 3b). The intensity ratio of these two peaks (I_D/I_G) is related to the degree of graphitization, porosity, and N and O doping of carbon materials. As shown in Figure 3c, the I_D/I_G value of NOPC-800 (1.21) is higher than that of NOPC-600 (1.09), NOPC-700 (1.16), and NOPC-900 (1.08), indicating that this sample has a large number of structural defects, which play an important role in energy storage. It is worth noting that a 2D peak was also observed at 2700 cm^{-1} for all samples, which is a secondary Raman scattering peak generated by the region boundary, indicating a high degree of graphitization in the samples. The nitrogen adsorption/desorption isotherms for the NOPC-600, NOPC-700, and NOPC-800 samples manifest a blend of type I and type IV isotherms, suggesting a porous architecture comprising abundant micropores and mesopores (Figure 3d). This structure offers ample buffer capacity for zinc ions, characterized by a larger hydration radius, as well as hydrogen ions with a smaller radius[5]. The isotherm of NOPC-900 is similar to type I, possibly due to the destruction of the original mesoporous structure of the material at excessive temperatures and the

DOI: 10.54254/2755-2721/63/20241005

etching of the carbon skeleton by zinc ions during the extensive reduction to elemental zinc. In contrast, NOPC-800 demonstrates the largest specific surface area of 1545.7 m^2 g^{-1}, ensuring not only sufficient active sites for ion storage but also a favorable rapid ion transport path. This characteristic is expected to result in excellent electrochemical performance.

3.3. Composition analysis of NOPC-800 sample

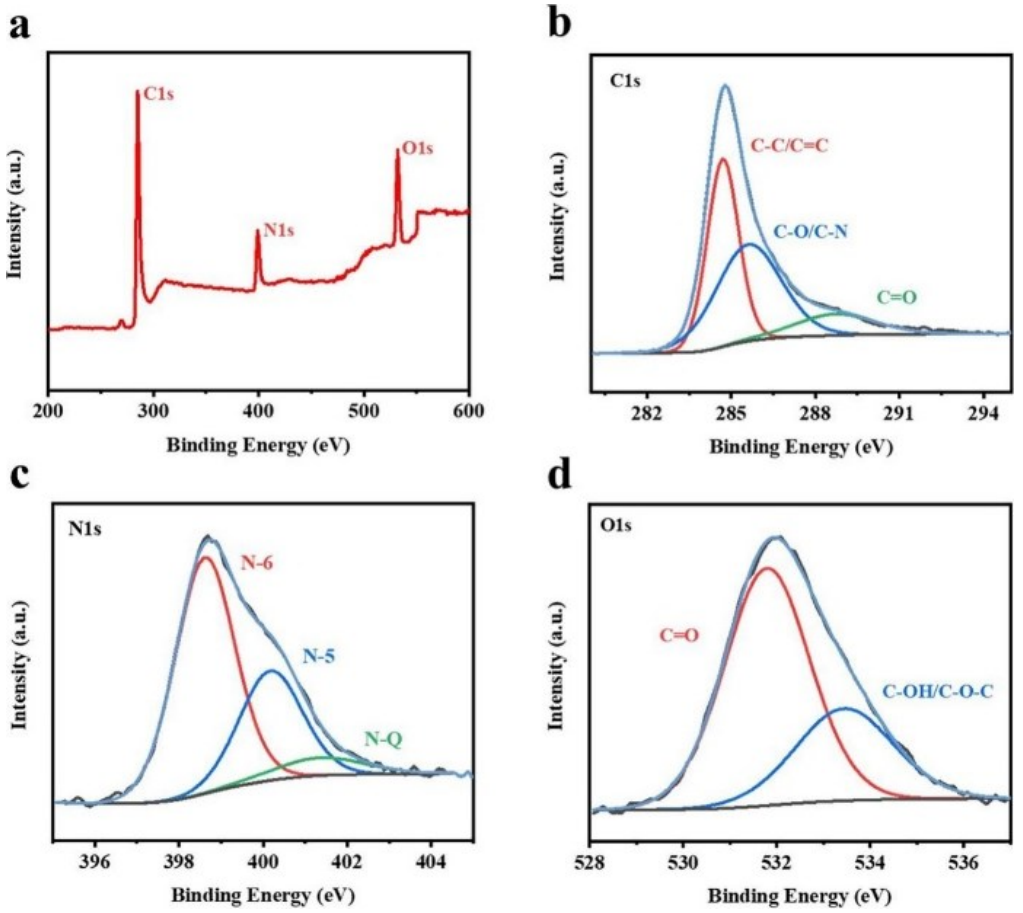

Figure 4. XPS pattern of NOPC-800. (a) Full spectrum, (b) O1s spectrum, (c) N1s spectrum, (d) C1s spectrum.

XPS was used to analyze elemental content and surface bonding patterns in NOPC-800. The prepared carbon materials are primarily composed of three elements: C, N, and O (Figure 4a), indicating the successful doping of nitrogen and oxygen into the carbon skeleton. Through calculation and analysis of the integrated area, it was determined that the nitrogen content in the NOPC-800 is 12.3 at%, while the oxygen content is 13.35 at%. The substantial increase in nitrogen and oxygen doping levels plays a pivotal role in altering the charge redistribution within the material and augmenting the pseudocapacitive reaction on the material surface, thereby accelerating ion reaction kinetics. The high-resolution C1s spectrum of NOPC-800 reveals three distinct peaks at 284.7, 285.6, and 288.7 eV, corresponding to C-C/C=C, C-O/C-N, and C=O in the aromatic ring, respectively (Figure 4b). Moving to the N1s spectrum, three peaks at 398.6, 400.2, and 402.3 eV are observed, corresponding to N-6 (pyridine nitrogen), N-5 (pyrrole nitrogen), and N-Q (graphitic nitrogen), with relative contents of 59.7%, 38.6%, and 1.7%, respectively (Figure 4c). The abundant N-6 and N-5 groups can serve as active sites for reversible redox reactions with electrolyte ions, while N-Q is crucial for enhancing the intrinsic conductivity of carbon materials. In the O1s spectrum, two peaks are identified at 531.8 eV (C=O) and 533.4 eV (C-OH/C-O-

DOI: 10.54254/2755-2721/63/20241005

C) with relative atomic percentages of 69.13% and 30.87%, respectively (Figure 4d). The integration of a substantial quantity of oxygen-rich functional groups serves to facilitate electrolyte penetration and enhance surface wettability. Simultaneously, the uniformly distributed high nitrogen content effectively reduces the adsorption energy barrier for zinc ions and hydrogen ions through the oxygen-containing functional groups on the material's surface[6], thereby promoting chemical adsorption.

3.4. Electrochemical performance of NOPC sample

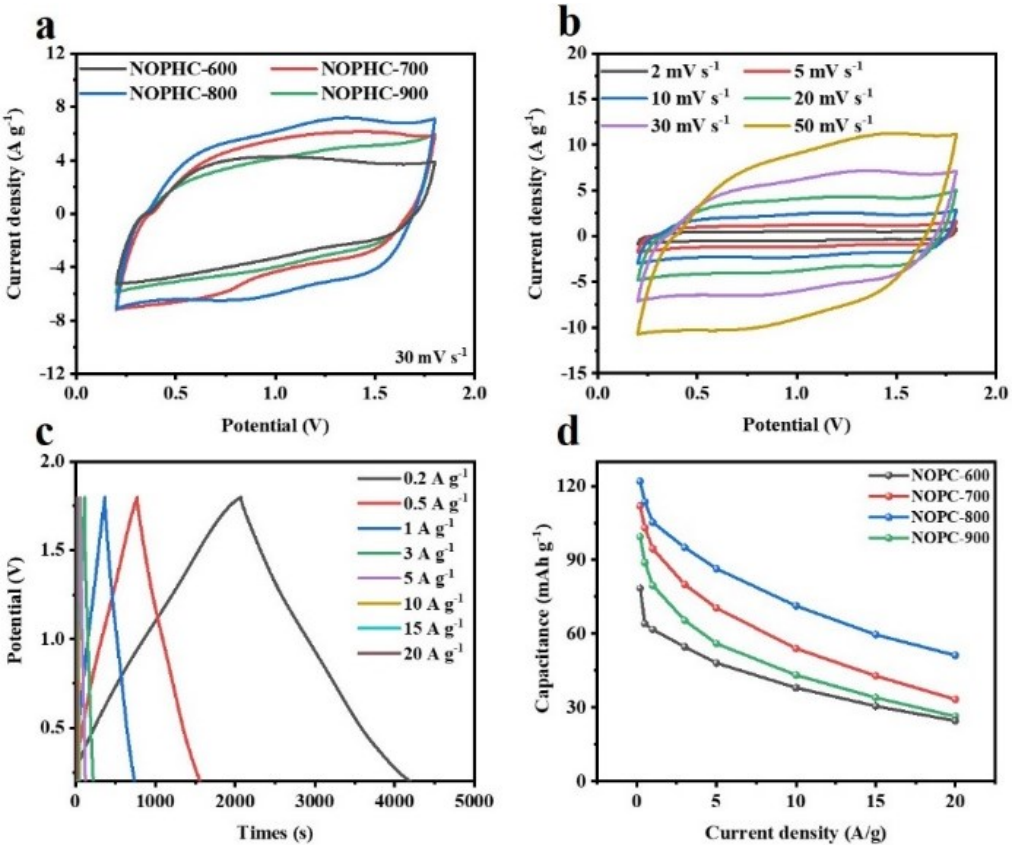

Figure 5. Electrochemical properties of ZISCs. (a) CV curves of NOPC-600, NOPC-700, NOPC-800 and NOPC-900 at a sweep speed of 30 mV s^{-1}, (b) CV curves of NOPC-800 at sweep speeds from 2 to 50 mV s^{-1}, (c) GCD curves of NOPC-800 at current density from 0.2 to 20A g^{-1}, (d) Rate performance diagram of NCOP-600, NOPC-700, NOPC-800 and NOPC-900.

Figure 5a depicts the cyclic voltammetry (CV) curve of ZISCs at a scan rate of 30 mV s-1. The quasi-rectangular shape suggests typical capacitive energy storage behavior, with the broad peak indicating the potential involvement of Faradaic redox reactions during the charge storage process, likely associated with the functional groups on the material surface[7]. In comparison to other samples, NOPC-800 exhibits the largest CV integration area, correlating with superior capacitance. Figure 5b illustrates the CV curves of NOPC-800 at different scan rates (2 mV s^{-1} to 50 mV s^{-1}). Notably, as the scan rate increases to 50 mV s^{-1}, there is no significant deformation in the CV curve, indicating favorable rate performance of the material. Furthermore, the galvanostatic charge-discharge (GCD) curves of NOPC-800 at various current densities (0.2-20 A g^{-1}) appear predominantly linear with no distinct plateaus, suggesting that the physical adsorption/desorption of zinc ions is the primary reaction mechanism (Figure 5c). Rate capability is a crucial metric for assessing material performance. Figure 5d summarizes the specific capacities of the samples at different current densities. Compared to NOPC-600 (99.4 mAh g^{-1}, 26.4 mAh g^{-1}), NOPC-700 (111.8 mAh g^{-1}, 33.3 mAh g^{-1}), and NOPC-900 (78 mAh g^{-1}, 24.6 mAh

DOI: 10.54254/2755-2721/63/20241005

g^{-1}), NOPC-800 exhibits a significant advantage. At a current density of 0.2 A g^{-1}, it achieves a specific capacity of 121.9 mAh g^{-1}, and even at a high current density of 20 A g^{-1}, the specific capacity reaches 51.2 mAh g^{-1}, retaining 42.0% of its initial capacity.

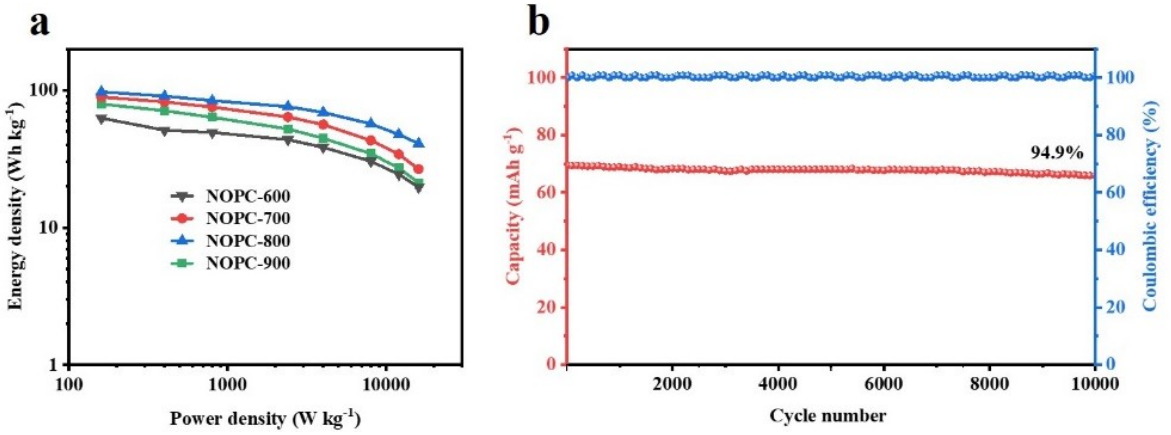

Figure 6. (a) Power density-energy density comparison chart of the sample, (b) Cycling performance chart of NOPC-800 at 10 A g^{-1}.

Figure 6a presents a comparative chart of power density and energy density among different samples. Notably, NOPC-800 exhibits remarkable performance with an energy density of 97.5 Wh kg^{-1} at a power density of 160 W kg^{-1}. Even under an exceptionally high power density of 16000 W kg^{-1}, NOPC-800 maintains a noteworthy energy density of 41 Wh kg^{-1}. Long cycling stability is a critical consideration for practical applications of zinc-ion supercapacitors. Following 10000 cycles at 10 A g^{-1}, NOPC-800 demonstrates outstanding performance, retaining 94.9% of its initial capacity, and achieving a Coulombic efficiency approaching 100% (Figure 6b).

4. Conclusion

In conclusion, we have successfully synthesized hierarchically porous carbon with high N/O co-doping using a one-pot method, resulting in a remarkable specific surface area of 1545.7 m^2 g^{-1}. This not only facilitates the infiltration of electrolyte ions but also provides abundant storage space for ions, thereby accelerating ion reaction kinetics. Benefiting from the synergistic effects of N/O co-doping and the substantial specific surface area, ZISCs assembled with NOPC-800 as the positive electrode exhibit outstanding electrochemical performance. Specifically, they demonstrate an impressive specific capacity of 121.9 mAh g^{-1} at a current density of 0.2 A g^{-1}, accompanied by a maximum energy density of 94.5 Wh kg^{-1} and an exceptional power density of 16 kW kg^{-1}. Moreover, even after 10,000 cycles, the capacity retention remains high at 94.9%. This work not only advances the understanding of heteroatom enrichment in carbon materials but also provides a promising avenue for achieving enhanced electrochemical performance.

Acknowledgments

The authors gratefully acknowledge the financial support received from the Beijing Natural Science Foundation (Grant No. 2202050) and the National Natural Science Foundation of China (Grant No. 21111120074). The invaluable characterization data utilized in this study were generously provided by the Analysis & Testing Center of Beijing Institute of Technology.

References

[1] Liu Y, Wu L 2023 *Nano Energy* **109** 108290.
[2] Ganfoud N, Sene A, Haefele M, Marin-Laflèche A, Daffos B, Taberna P. L and Rotenberg B 2019 *Energy Storage Mater.* **21** 190-195.
[3] Wei F, Zeng Y, Guo Y, Li J, Zhu S, Gao S and He X 2023 *Chem. Eng. J.* **468** 143576.

DOI: 10.54254/2755-2721/63/20241005

[4] Wang L, Peng M, Chen J, Hu T, Yuan K and Chen Y 2022 *Adv. Mater.* **34(39)** 2203744.
[5] Jian W, Zhang W, Wei X, Wu B, Liang W, Wu Y and Qiu X 2022 *Adv. Funct. Mater.* **32(49)** 2209914.
[6] Wang L, Peng M, Chen J, Tang X, Li L, Hu T and Chen Y 2022 *ACS Nano* **16(2)** 2877-2888.
[7] Wang L, Huang M, Huang J, Tang X, Li L, Peng M and Chen Y. 2021. J. Mater. Chem. A **9(27)** 15404-15414.